AJNR

This information is current as of July 30, 2025.

Diagnostic Role of Diffusion-Weighted and Dynamic Contrast-Enhanced Perfusion MR Imaging in Paragangliomas and Schwannomas in the Head and Neck

Y. Ota, E. Liao, A.A. Capizzano, R. Kurokawa, J.R. Bapuraj, F. Syed, A. Baba, T. Moritani and A. Srinivasan

Diagnostic Role of Diffusion-Weighted and Dynamic Contrast-Enhanced Perfusion MR Imaging in Paragangliomas and Schwannomas in the Head and Neck

Y. Ota, E. Liao, A.A. Capizzano, R. Kurokawa, J.R. Bapuraj, F. Syed, A. Baba, T. Moritani, and A. Srinivasan

ABSTRACT

BACKGROUND AND PURPOSE: Distinguishing schwannomas from paragangliomas in the head and neck and determining succinate dehydrogenase (*SDH*) mutation status in paragangliomas are clinically important. We aimed to assess the clinical usefulness of DWI and dynamic contrast-enhanced MR imaging in differentiating these 2 types of tumors, as well as the *SDH* mutation status of paragangliomas.

MATERIALS AND METHODS: This retrospective study from June 2016 to June 2020 included 42 patients with 15 schwannomas and 27 paragangliomas (10 *SDH* mutation-positive and 17 *SDH* mutation-negative). ADC values, dynamic contrast-enhanced MRI parameters, and tumor imaging characteristics were compared between the 2 tumors and between the mutation statuses of paragangliomas as appropriate. Multivariate stepwise logistic regression analysis was performed to identify significant differences in these parameters.

RESULTS: Fractional plasma volume ($P \leq .001$), rate transfer constant ($P = .038$), time-to-maximum enhancement ($P < .001$), maximum signal-enhancement ratio ($P < .001$) and maximum concentration of contrast agent ($P < .001$), velocity of enhancement ($P = .002$), and tumor characteristics including the presence of flow voids ($P = .001$) and enhancement patterns ($P = .027$) showed significant differences between schwannomas and paragangliomas, though there was no significant difference in ADC values. In the multivariate logistic regression analysis, fractional plasma volume was identified as the most significant value for differentiation of the 2 tumor types ($P = .014$). ADC values were significantly higher in nonhereditary than in hereditary paragangliomas, while there was no difference in dynamic contrast-enhanced MR imaging parameters.

CONCLUSIONS: Dynamic contrast-enhanced MR imaging parameters show promise in differentiating head and neck schwannomas and paragangliomas, while DWI can be useful in detecting *SDH* mutation status in paragangliomas.

ABBREVIATIONS: AUC = area under the curve; DCE = dynamic contrast-enhanced; EES = extravascular extracellular space; Kep = rate transfer constant between EES and blood plasma per minute; K^{trans} = volume transfer constant between EES and blood plasma per minute; SDH = succinate dehydrogenase; SER = signal-enhancement ratio; TIC = time-intensity curve; TME = time-to-maximum enhancement; Ve = EES volume per unit tissue volume; Vp = blood plasma volume per unit tissue volume

Schwannomas are benign nerve sheath tumors arising from Schwann cells, and paragangliomas are neuroendocrine tumors arising from the autonomic system.[1,2] Both schwannomas and paragangliomas can occur in the head and neck region. On conventional MR imaging, schwannomas typically present as a homogeneously enhancing mass with cystic changes, whereas paragangliomas usually demonstrate heterogeneous enhancement with a "salt-and-pepper" appearance and necrotic or cystic changes.[3,4] When present, these classic imaging characteristics can help define these lesions, but a definitive diagnosis on imaging remains challenging, especially when these imaging characteristics are not present or overlap.

Moreover, conventional MR imaging and CT have been reported to be unable to identify the difference between nonhereditary and hereditary paragangliomas.[5] Hereditary paragangliomas are primarily related to mutations in the genes of succinate dehydrogenase (*SDH*), which are responsible for *SDH* subunits *A, B, C, D*, and *AF2 (SDHA, SDHB, SDHC, SDHD, SDHAF2)* proteins and play an important role in the mitochondria for energy production. For example, *SDHD* and *SDHB* mutations are related to multiplicity and malignancy, respectively,[1] and these associations make the differentiation of nonhereditary and hereditary paragangliomas highly important.

Schwannomas are histologically characterized by regions of high cellularity and fewer cells with cystic or xanthomatous changes, whereas paragangliomas mainly demonstrate nests of tumor cells separated by peripheral capillaries.[6,7] ADC values may
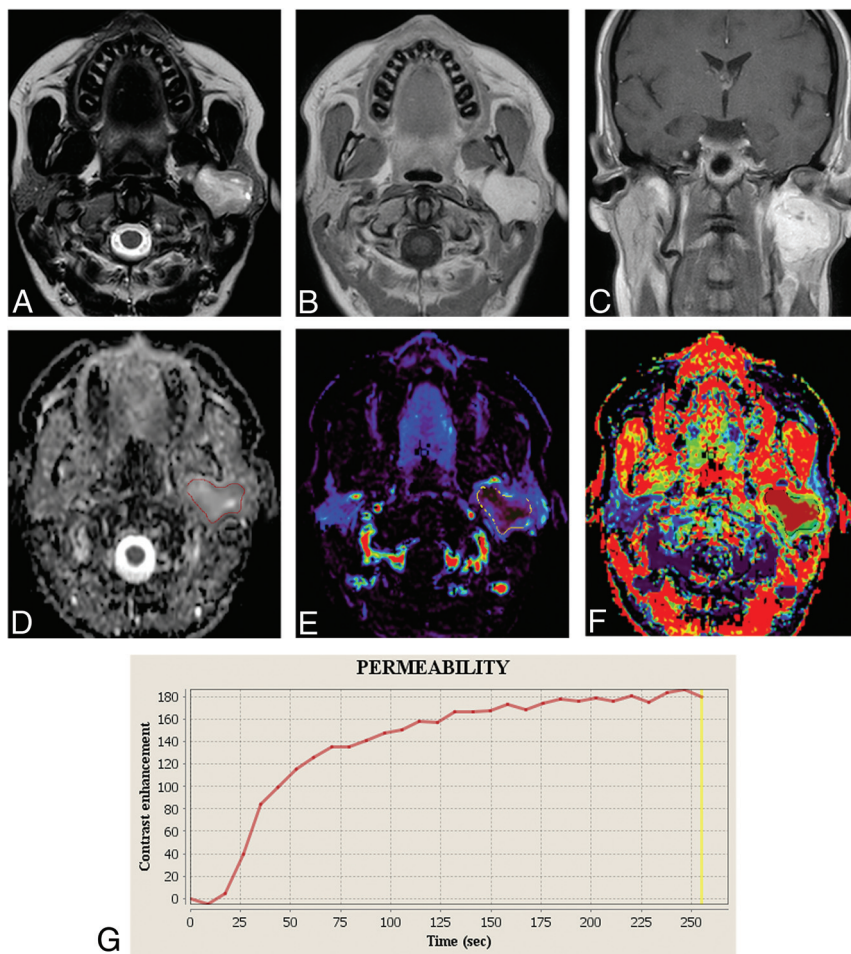
FIG 1. A 41-year-old woman with a schwannoma in the left parotid space. *A*, T2-weighted image shows a hyperintense mass in the left parotid gland. *B* and *C*, Contrast-enhanced T1-weighted image shows homogeneous enhancement. *D*, Mean ADC and normalized mean ADC are 1.15×10^{-3} mm²/s and 1.48, respectively. *E* and *F*, Vp and TME are demonstrated. *G*, The TIC demonstrates a low peak enhancement with a long time-to-peak.

contribute to their imaging differentiation on the basis of these histopathologic differences. Also, dynamic contrast-enhanced (DCE)-MR imaging can assess tumor microvasculature and permeability[8,9] and has been increasingly used to assess head and neck lesions.[10-13] However, DWI and DCE-MR imaging analysis for these tumors and for the mutation status of paragangliomas has not been fully explored. This study was designed to test the hypothesis that ADC values and DCE-MR imaging could help differentiate schwannomas from paragangliomas and distinguish nonhereditary and hereditary paragangliomas.

MATERIALS AND METHODS
Study Population
Our institutional review board approved this retrospective single-center study and waived the requirement for informed consent. Data were acquired in compliance with all applicable Health Insurance Portability and Accountability Act regulations.

We retrospectively reviewed the medical records of 775 patients from June 2016 to June 2020 with suspected head and neck tumors

in a single center. There were 97 pathologically proved schwannomas and 36 paragangliomas in the head and neck. DCE-MR imaging was performed when head and neck malignancy was suspected or the lesions required further characterization. Patients who did not have pretreatment conventional MR imaging or DCE-MR imaging ($n = 72$); had been previously treated by surgery, embolization, or radiation therapy ($n = 15$); or did not have genetic testing for *SDH* mutations for paragangliomas ($n = 4$) were excluded. Genetic testing was performed by the PGLNext panel (Ambry Genetics), which requires collecting blood or saliva samples by an appropriate kit and analyzes 12 genes including *SDH* subunits *SDHA, SDHAF2, SDHB, SDHC,* and *SDHD*. This test was designed and validated to detect >99.9% of the gene mutations noted above.

In total, 42 patients (12 men, 30 women; 46.0 [SD, 16.5] years of age; range, 18–70 years of age) with 15 schwannomas and 27 paragangliomas (10 *SDH* mutation-negative, 17 *SDH* mutation-positive) were included in this study.

MR Imaging Acquisition
MR imaging examinations were performed using 1.5T ($n = 30$) and 3T ($n = 12$) scanners (Ingenia; Philips Healthcare). They were performed with a 16-channel Neurovascular coil (Stryker) with the patient in the supine position. Acquired sequences included axial T1WI and T2WI, axial and coronal contrast-enhanced fat-saturated T1WI, and DWI using echo-planar imaging with the following DWI parameters: TR range = 5000–10,000 ms; TE range = 58–106 ms; number of excitations = 1, 2; section thickness/gap = 3.5–4/0–1 mm; FOV = 220–260 mm; matrix size = 128–200 × 128–200; and 3 diffusion directions. Sensitizing diffusion gradients were applied sequentially with b-values of 0 and 1000 s/mm².

The DCE-MR imaging sequence was performed using 3D T1-weighted fast-field echo images, with the administration of gadobenate dimeglumine contrast (MultiHance; Bracco Diagnostics). An intravenous bolus of 20 mL of gadobenate dimeglumine was administered using a power injector with a flow rate of 5.0 mL/s through a peripheral arm vein, followed by a 20-mL saline flush. DCE-MR imaging was sequentially performed for 30 dynamic phases. These techniques were performed for all patients in a single center.

The parameters of 3D T1 fast-field echo were as follows: TR = 4.6 ms, TE = 1.86 ms, flip angle = 30°, section thickness =
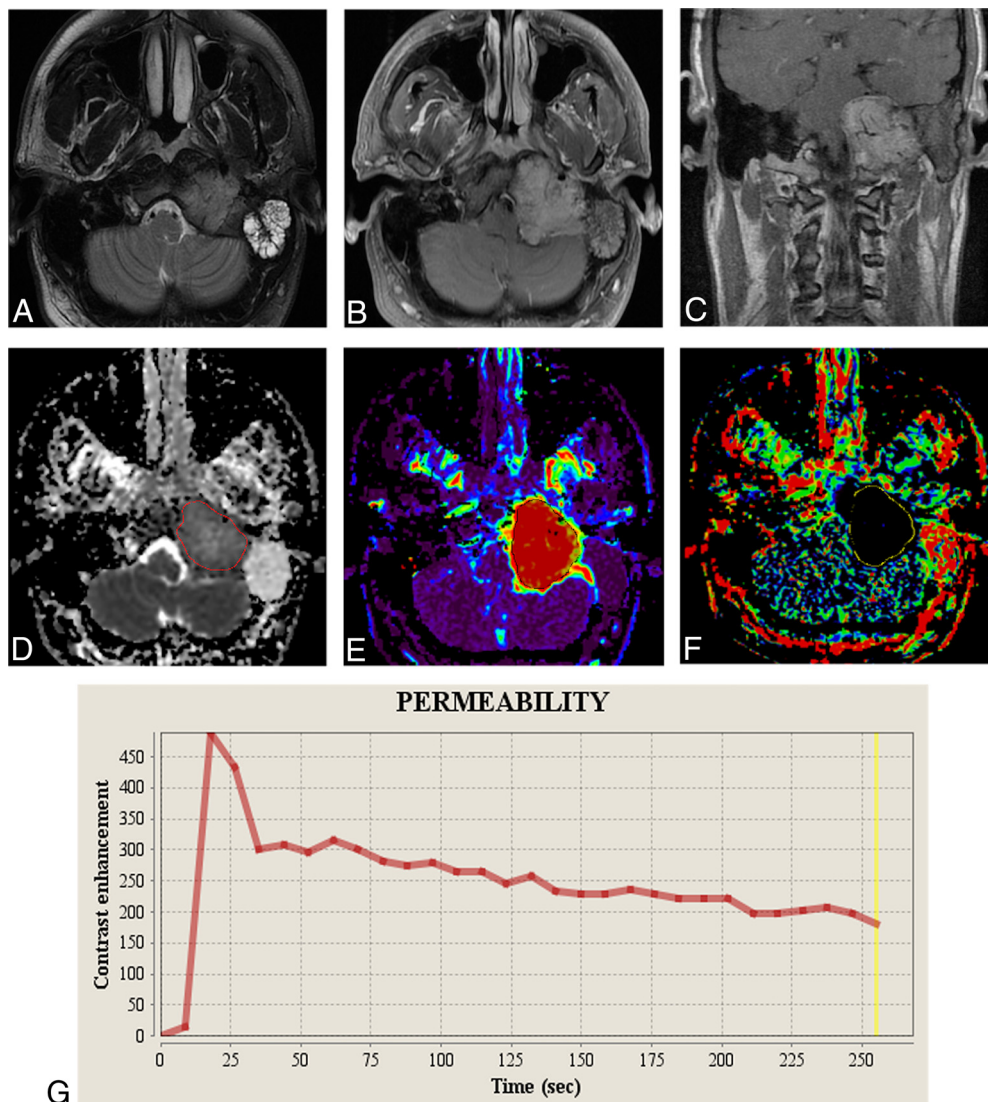
FIG 2. A 26-year-old man positive for the *SDHB* mutation with a paraganglioma in the left jugular foramen. *A*, T2-weighted image shows a heterogeneous irregular mass in the left jugular foramen. *B* and *C*, Contrast-enhanced T1-weighted images show a heterogeneous, enhancing mass with a vascular flow void. *D*, Mean ADC and normalized mean ADC are 1.12×10^{-3} mm^2/s and 1.48. *E* and *F*, Vp and TME are demonstrated. *G*, The TIC demonstrates a higher peak enhancement with a shorter time-to-peak compared with Fig 1.

5.0 mm, FOV = 240×240 mm^2, voxel size = $1.0 \times 1.0 \times 5.0$ mm^3, number of excitations = 1, number of slices per dynamic scan = 48, temporal resolution = 8.4 seconds, and total acquisition time of 4 minutes 13 seconds using a 16-channel Neurovascular coil.

Data Analysis

Tumor Characteristics. All conventional MR images were reviewed independently by 2 board-certified radiologists with 7 and 10 years of experience in neuroradiology, respectively. They were blinded to clinical information, imaging results from other modalities, and histopathologic results. Both radiologists evaluated imaging characteristics using the following metrics:

1) Maximum axial diameter of the tumor was evaluated on postcontrast T1-weighted images

2) Presence of flow voids, cystic or necrotic changes, and enhancement pattern (homogeneous or heterogeneous pattern),

evaluated on T1-weighted, T2-weighted, and pre- and postcontrast fat-saturated T1-weighted images. These were recorded as binary variables. Cystic changes were defined as the following: nonenhancing, predominantly T1 hypointense and T2 hyperintense areas; necrotic changes were defined as nonenhancing, predominantly T1 hypointense and heterogeneously T2 hyperintense areas; and flow voids were defined as nonenhancing T1 hypointense, T2 hypointense vessel structures within the tumors (Figs 1A–C and 2A–C).

3) As for location (percentage of head lesion/head and neck lesion), jugular foramen and jugulotympanicum lesions were classified into the head location, and carotid space and parotid space lesions were classified into the neck location.

ADC Analysis. ADC maps were constructed by a monoexponential fitting model using commercially available software (Olea Sphere, Version 3.0; Olea Medical). The radiologist with 7 years'

experience carefully outlined the lesions using freehand ROIs (Figs 1*D* and 2*D*) and transposed the ROIs to the ADC map. When geometric distortion was observed, the location and size were adjusted on the ADC map so that the ROI would be included in the tumor. The ROIs encompassed predominantly solid, enhancing portions of tumors without cystic or necrotic areas on postcontrast T1-weighted images. Additionally, ROIs spared the peripheral 2 mm of lesions to avoid volume averaging.[14] As an internal standard, an ROI was placed within the cervical spinal cord at the level of the C2–C3 disc space, which was included in the FOV of every study.[15] A normalized ADC ratio was calculated by dividing each mean ADC value of the lesion by the mean ADC value of the cervical cord to adjust for variation of ADC values across MR imaging scanners, magnetic field strengths, and matrix sizes.

Quantitative DCE-MR Imaging Analysis. All quantitative analyses in DCE-MR imaging were performed using the Olea Sphere 3.0 software Permeability Module, which is based on the extended Tofts model, by which pixel-based parameter maps are calculated from time-intensity curves (TICs) (Figs 1 *E–G* and 2*E–G*). The radiologist with 7 years' experience placed the ROIs on the permeability maps, predominantly including the enhancing components of the tumors without cystic or necrotic areas. Manual ROIs spared the peripheral 2 mm of lesions to avoid volume averaging. An ROI was placed at the external carotid artery of the affected side for the arterial input function. The calculated quantitative parameters were blood plasma volume per unit tissue volume (V_p), extravascular extracellular space (EES) volume per unit tissue volume (V_e), volume transfer constant between EES and blood plasma per minute (K^{trans}), and rate transfer constant between EES and blood plasma per minute (K_{ep}).

Semiquantitative DCE-MR Imaging Analysis. Semiquantitative analysis was performed using the same ROIs described above with the Olea Sphere 3.0 software Permeability Module. The average signal intensity within the ROI was plotted against time, and TICs were constructed. The following parameters were calculated on a pixel-by-pixel basis from the TICs: area under the curve (AUC, the relative quantity of contrast agent over time), maximum concentration of contrast agent (peak enhancement), velocity of enhancement (wash-in), velocity of enhancement loss (washout), maximum signal-enhancement ratio (SER), and time-to-maximum enhancement (TME).

Statistical Analysis

Patient demographics including age and sex; the number of lesions; tumor characteristics including the maximum diameter of tumors and the presence of vascular flow voids; the presence of cystic or necrotic change; enhancement patterns (homogeneous or heterogeneous pattern); and location (percentage of head lesions/head and neck lesions) were compared between the 2 types of tumors and between *SDH* mutation-positive and *SDH* mutation-negative paragangliomas.

Age was compared using a *t* test and described as mean (SD). The maximum diameter of the tumor was compared using the Mann-Whitney *U* test. The binary variables such as sex (ratio of male to female), the presence of vascular flow voids, the presence of cystic or necrotic change, enhancement patterns, and location (the percentage of head lesions/head and neck legions) were compared using the Fisher exact test.

For statistically significant tumor characteristics, AUCs were evaluated from the receiver operating characteristic analysis.

Mean ADC and normalized mean ADC (mean ADC divided by the ADC of the cervical cord) were compared between paragangliomas and schwannomas using a *t* test. Additionally, mean ADC and normalized mean ADC were also compared between *SDH* mutation-negative and *SDH* mutation-positive paragangliomas. Quantitative parameters and semiquantitative parameters were compared between schwannomas and paragangliomas and between *SDH* mutation-negative and *SDH* mutation-positive paragangliomas using the Mann-Whitney *U* test.

For values that showed statistically significant differences in ADC values, quantitative parameters, and semiquantitative parameters, the optimal cutoff values in receiver operating characteristic analysis were determined as a value to maximize the Youden index (sensitivity + specificity–1). On the basis of the cutoff values, the diagnostic performances (sensitivity, specificity, positive predictive value, negative predictive value, and accuracy) were calculated.

Multivariate stepwise logistic regression analysis was performed to identify the most significant parameter to distinguish schwannomas and paragangliomas using the forward stepwise selection method. For this method, the values with a *P* value of < .05 according to the univariate analysis were used.

Interreader agreement for tumor characteristics was assessed using the κ coefficient, which was interpreted as follows: <0.40, poor-to-fair agreement; 0.41–0.60, moderate agreement; 0.61–0.80, substantial agreement; and 0.81–1.00, almost perfect agreement.[16]

All statistical calculations were conducted with JMP Pro, Version 15.0.0 (SAS Institute). Variables with a *P* value <.05 were considered statistically significant.

RESULTS

The patient demographic and tumor characteristics are shown in Table 1.

There was no significant difference in age or sex ($P = .27$ and .73) between those with schwannomas and those with paragangliomas. Regarding tumor characteristics, the presence of vascular flow voids and the enhancement pattern (homogeneous or heterogeneous pattern) revealed significant differences between paragangliomas and schwannomas ($P = .001$ and .027, respectively). The AUCs of the presence of vascular flow voids and enhancement patterns were 0.77 (95% CI, 0.64–0.89) and 0.69 (95% CI, 0.53–0.84), respectively. Schwannomas were located at the jugular foramen ($n = 5$), carotid space ($n = 6$), and parotid space ($n = 4$). Paragangliomas included the glomus jugulare ($n = 8$), glomus jugulotympanicum ($n = 3$), and carotid body paraganglioma ($n = 16$). There was no significant difference in location (head lesions/head and neck lesions) between the 2 tumors (schwannomas: 11/27 versus paragangliomas: 5/15; $P = .75$).

There were 10 *SDH* mutation-negative and 17 *SDH* mutation-positive paragangliomas (*SDHA*: 1, *SDHB*: 8, *SDHC*: 2, *SDHD*: 6).

Table 1: Patient demographics and tumor characteristics in schwannomas and paragangliomas[a]

	Schwannomas (n = 15)	Paragangliomas (n = 27)	P Value
No.	15	27	NA
Sex (male/female)	5:10	7:20	.73
Age (yr)	42.2 (SD, 15.1)	48.2 (SD, 17.2)	.27
Maximum diameter (mm)	31.4 (SD, 15.4)	32.3 (SD, 15.6)	.76
Presence of vascular flow voids (salt-and-pepper appearance)	2/15	18/27	.001[b]
Cystic or necrotic change	5/15	14/27	.34
Enhancement pattern (homogeneous enhancement/total)	10/15	8/27	.027[b]
Location (head lesion/total)	5/15	11/27	.75

Note:—NA indicates not applicable.
[a] Values are mean (SD).
[b] $P < .05$.

Table 2: ADC values and DCE-MR imaging dynamic parameters of schwannomas and paragangliomas[a]

	Schwannomas (n = 15)	Paragangliomas (n = 27)	P Value
Mean ADC ($\times 10^{-3}$ mm^2/s)	1.17 (SD, 0.31)	1.12 (SD, 0.26)	.56
Normalized mean ADC	1.54 (SD, 0.43)	1.45 (SD, 0.37)	.53
Quantitative values			
Vp	0.06 (0.03–0.12)	0.40 (0.34–0.54)	<.001[b]
Ve	0.42 (0.25–0.77)	0.28 (0.16–0.47)	.38
Kep (min^{-1})	0.58 (0.36–0.67)	1.02 (0.43–2.27)	.038[a]
K^{trans} (min^{-1})	0.15 (0.11–0.26)	0.31 (0.13–0.74)	.16
Semiquantitative values			
AUC (mmol.min/L)	5.6×10^4 (1.95×10^4 –1.55×10^5)	7.0×10^4 (3.8×10^4 –4.1×10^5)	.08
Peak enhancement	137 (75–220)	294 (266–300)	<.001[b]
Wash-in	1.4 (0.74–3.8)	7.26 (2.54–42.6)	.002[b]
Washout	3.4 (0.77–8.4)	1.0 (0.42–6.0)	.35
SER	53.9 (47–90)	146 (112–211)	<.001[b]
TME (sec)	160 (108–239)	36.2 (27.7–77.4)	<.001[b]

[a] The numbers in parentheses represent interquartile range.
[b] $P < .05$.

Between *SDH* mutation-negative and mutation-positive paragangliomas, age was higher in *SDH* mutation-negative paragangliomas than in *SDH* mutation-positive paragangliomas (56.8 [SD, 12.9] years versus 43.1 [SD, 17.7] years; $P = .043$). There were no significant differences in other demographics and tumor characteristics (male/female: 1:9 versus 6:1; $P = .20$; maximum diameter: 36.2 [SD, 21.5] mm versus 28.6 [SD, 10.2] mm; $P = .22$; presence of vascular flow voids [salt-and-pepper appearance]: 6/10 versus 12/17; $P = .68$; percentage of cystic or necrotic changes: 5/10 versus 9/17; $P = 1.0$; enhancement pattern [homogeneous enhancement/total]: 4/10 versus 4/17; $P = .42$; location [head lesion/total]: 5/10 versus 6/17; $P = .69$).

Interreader agreement for tumor characteristics showed almost perfect agreement ($\kappa = 0.85$–0.89).

For schwannomas and paragangliomas, Table 2 summarizes the results of ADCs and dynamic perfusion data. There were no significant differences in mean ADC and normalized mean ADC between schwannomas and paragangliomas ($P = .56$ and 0.46, respectively). The mean ADC value of the cervical cord, used as an internal standard, was 0.77 (SD, 0.05) $\times 10^{-3}$ mm^2/s. Regarding

quantitative DCE parameters, Vp (schwannomas versus paragangliomas; median, 0.06, versus 0.40; $P = <.001$) and Kep (median, 0.58, versus 1.02; $P = .038$) showed significant differences. Arterial input function curves showed the pulsed input pattern in all patients. Among semiquantitative parameters, TME (median, 160, versus 36.2; $P < .001$), SER (median, 53.9, versus 146; $P < .001$), peak enhancement (median, 137, versus 294; $P < .001$), and wash-in (median, 1.40, versus 7.26; $P = .002$) showed significant differences between schwannomas and paragangliomas. Representative cases of DCE-MR imaging analysis are shown in Figs 3 and 4.

The diagnostic performance of Vp, Kep, TME, SER, peak enhancement, and wash-in are shown in Table 3, and receiver operating characteristic curves of Vp, TME, and peak enhancement, in Fig 5. The AUCs of Vp and TME offered the best performance of the quantitative and semiquantitative perfusion parameters, respectively. In the multivariate logistic regression analysis for differentiating schwannomas and paragangliomas from ADCs, DCE-MR imaging parameters, and tumor characteristics, Vp was identified as the most significant variable in the differentiation of these 2 tumors ($P = .014$).

As for *SDH* mutation-negative and *SDH* mutation-positive paragangliomas, mean ADC and normalized mean ADC were significantly higher in *SDH* mutation-negative paragangliomas than in *SDH* mutation-positive paragangliomas (mean ADC: 1.27 [SD, 0.18] versus 1.04 [SD, 0.26] $\times 10^{-3}$ mm^2/s; $P = .023$; normalized mean ADC: 1.73 [SD, 0.32] versus 1.31 [SD, 0.31]; $P < .001$, respectively). The diagnostic performances of mean ADC and normalized mean ADC demonstrated sensitivities of 0.82 and 0.88, specificities of 0.89 and 0.78, positive predictive values of 0.93 and 0.88, negative predictive values of 0.73 and 0.78, accuracy of 0.85 and 0.85, and AUCs of 0.83 and 0.87, with cutoff values of 1.14×10^{-3} mm^2/s and 1.52, respectively.

Regarding DCE-MR imaging analysis of *SDH* mutation-negative and *SDH* mutation-positive paragangliomas, there were no perfusion parameters that showed statistical significance (Vp: median, 0.36 versus 0.41; $P = .68$; Ve: median, 0.33 versus 0.28; $P = .89$; Kep: median, 1.2 versus 0.90 minute^{-1}; $P = .53$; K^{trans}: median, 0.28 versus 0.31 minute^{-1}; $P = 1.0$; AUC: median, 6.6×10^4 versus 2.3×10^5 mmol.min/L; $P = .90$; peak enhancement: median, 287 versus 297; $P = .96$; wash-in: median, 5.5 versus 9.6; $P = .67$; washout: median, 1.0 versus 1.2; $P = .98$; SER: median, 150 versus 142; $P = .54$; TME: median, 46.4 versus 36.1; $P = .98$).
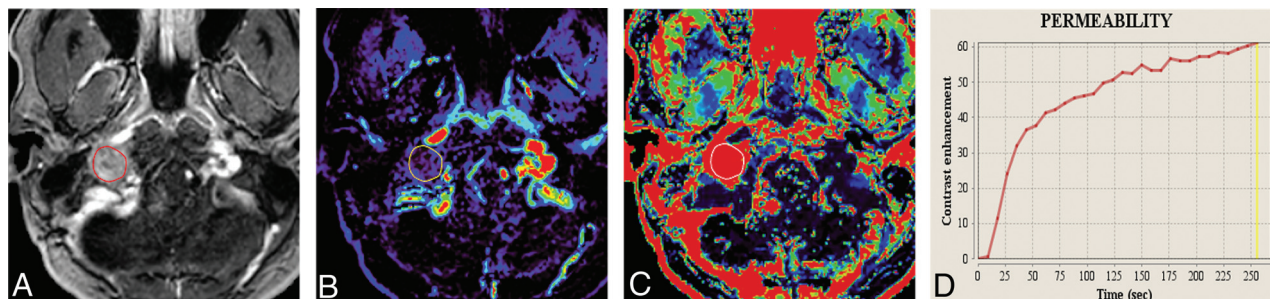
FIG 3. A 34-year-old woman with a schwannoma in the right jugular foramen. *A*, The permeability map shows a heterogeneously enhancing mass in the right jugular foramen. *B* and *C*, The values of Vp and TME are 0.03 and 219, respectively. *D*, The TIC demonstrates a low peak enhancement with a long time-to-peak compared with Fig 2.
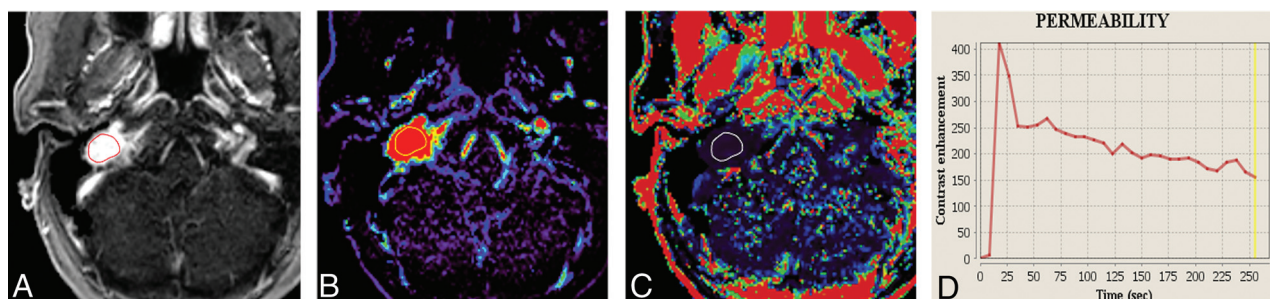

FIG 4. A 70-year-old man negative for the *SDH* mutation with a paraganglioma in the right jugular foramen. *A*, The permeability map shows a homogeneously enhancing mass in the right jugular foramen. *B* and *C*, The values of Vp and TME are 0.53 and 27.7, respectively. *D*, The TIC demonstrates a high peak enhancement with a short time-to-peak compared with Figs 1 and 3.

Table 3: Diagnostic performance of dynamic parameters in differentiating schwannomas and paragangliomas

	Vp	Kep	Peak Enhancement	Wash-In	SER	TME (Sec)
Cutoff	0.30	0.86	277	6.29	135	62.8
Sensitivity	0.91	0.67	0.74	0.63	0.89	0.72
Specificity	1.00	0.87	1.00	0.93	0.73	1.00
PPV	1.00	0.90	1.00	0.94	0.86	1.00
NPV	0.88	0.59	0.68	0.58	0.79	0.68
Accuracy	0.95	0.74	0.83	0.74	0.83	0.83
AUC	0.99	0.70	0.89	0.80	0.86	0.92

Note:—PPV indicates positive predictive value; NPV, negative predictive value.

DISCUSSION

This retrospective study aimed to evaluate the clinical usefulness of DWI and DCE-MR imaging parameters to differentiate head and neck schwannomas and paragangliomas and distinguish *SDH* mutation status in paragangliomas. DCE-MR imaging parameters identified significant statistical differences between schwannomas and paragangliomas with AUCs of 0.70–0.99, though no significant differences in ADC values were identified. Vp was the most promising parameter to differentiate the 2 tumor types. Within the paraganglioma subgroup, *SDH* mutation-negative paragangliomas showed higher mean and normalized mean ADC values than *SDH* mutation-positive paragangliomas with AUCs of 0.88 and 0.92, while DCE-MR imaging parameters failed to show any significant differences. Regarding tumor characteristics, as previous studies have reported, the presence of flow voids and the enhancement pattern showed significant differences between schwannomas and paragangliomas, while age was younger in *SDH* mutation-positive than *SDH* mutation-negative paragangliomas.[1,3,4]

Semiquantitative parameters are based on and calculated from TICs, which can differentiate divergent hemodynamic patterns. In our study, TME, SER, peak enhancement, and wash-in showed significant differences between the 2 tumors. Paragangliomas showed higher peak enhancement and SER, with a shorter TME and greater wash-in than schwannomas. TME showed the most significant difference between the 2 tumors with an AUC of 0.92. Pathologically, paragangliomas typically show chief cells forming variably sized clusters with a capillary network that primarily functions as an arteriovenous shunt,[17] while schwannomas show focal clusters of vascular proliferation with extensive hyalinization.[18] These histologic differences are suspected to underlie the divergent hemodynamic patterns between the 2 tumors.

Quantitative parameters were calculated on the basis of the extended Tofts model, which reflects the microcirculation within the lesion.[19] In our study, Vp and Kep were significantly higher in paragangliomas than in schwannomas, and Vp showed the most significant difference between the 2 tumors with an AUC of 0.99 at a cutoff of 0.30 seconds. Vp is defined as blood plasma
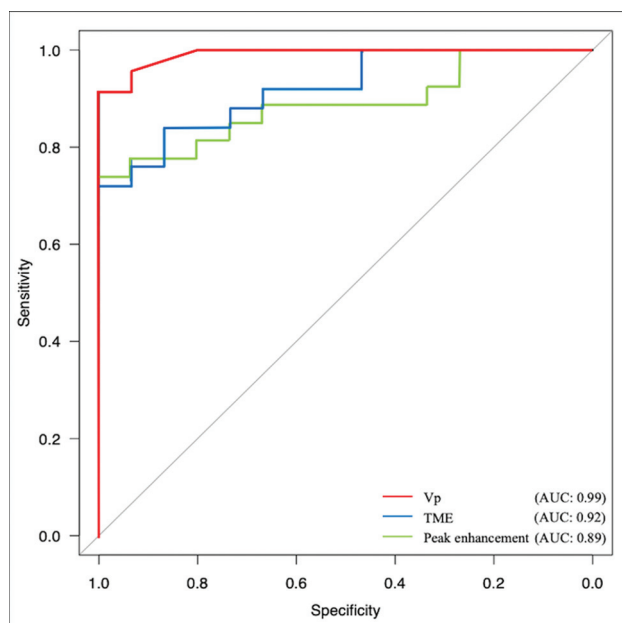
FIG 5. Receiver operating characteristic curves of Vp, TME, and peak enhancement. The AUCs of Vp, TME, and peak enhancement were 0.99, 0.92, and 0.89 with cutoff values of 0.30, 62.8, and 277 seconds, respectively.

volume per unit tissue volume, which may represent vascularity within the tumor, and Kep is defined as rate transfer of constant between EES and blood plasma per minute, which represents permeability.[20] Our results indicate that DCE-MR imaging can be used to differentiate schwannomas from paragangliomas on the basis of their disparate hemodynamic patterns and microcirculation, further refining our ability to differentiate these tumors on imaging.

There were no significant differences in DCE-MR imaging parameters when comparing *SDH* mutation-negative and mutation-positive paragangliomas in this study. Published literature evaluating potential differences in the vascularity or permeability of paragangliomas based on *SDH* mutation status is lacking. However, the results of this study indicate that there may be no significant difference in the microcirculation of paragangliomas based on *SDH* mutation status.

ADC analysis did not identify any significant differences between schwannomas and paragangliomas; however, it demonstrated significant differences between *SDH* mutation-negative and mutation-positive paragangliomas. Histologically, paragangliomas have been recognized as showing various tumor cell morphology and cellularity and a variety of histologic patterns,[21] including chief cells forming variable-sized clusters. A previous study suggested that the histopathologic background of paragangliomas may differ depending on *SDH* mutation status; this potential divergence in histology may account for the visualized differences in ADC values,[5] though correlative histologic studies are lacking. Schwannomas demonstrate a biphasic pattern of high cellularity, and fewer cells with cystic or xanthomatous changes.[7] Previously, it has been reported that schwannomas exhibit a wide range of ADC values (0.74 [SD, 0.08] to 2.08 [SD, 0.33] $\times 10^{-3}$ mm^2/s),[14] which could be due to the differences in

internal structures such as cystic or xanthomatous changes as mentioned above. Given that there were no differences in ADC values between the 2 tumor types, even despite avoiding cystic or necrotic components of the tumors when drawing ROIs, DWI may not reliably differentiate these tumors.

Our study had several limitations. First, this was a retrospective study and included a relatively small population from a single institution. Second, DCE-MR imaging was performed using both 1.5T and 3T scanners, which may add heterogeneity to the calculated perfusion parameters. Third, in DCE-MR imaging analysis, there could be a potential bias influenced by the previous knowledge of the morphologic findings of the tumors, even though the reader was blinded to the pathologic results. Finally, in our institution, genetic testing is recommended for all the patients who are clinically or radiologically suspected of having hereditary paragangliomas, so prior probability of genetic mutation in our study population may be higher than in the overall population.

CONCLUSIONS

DCE-MR imaging can provide promising noninvasive parameters that can be used to differentiate schwannomas and paragangliomas in the head and neck when the differential diagnosis is challenging. Vp is the most promising value to differentiate the 2 tumors. DWI can be useful to distinguish *SDH* mutation status in paragangliomas.

REFERENCES

1. Withey SJ, Perrio S, Christodoulou D, et al. **Imaging features of succinate dehydrogenase-deficient pheochromocytoma-paraganglioma syndromes.** *Radiographics* 2019;39:1393–1410 CrossRef Medline
2. Biswas D, Marnane CN, Mal R, et al. **Extracranial head and neck schwannomas–a 10-year review.** *Auris Nasus Larynx* 2007;34:353–59 CrossRef Medline
3. Woolen S, Gemmete JJ. **Paragangliomas of the head and neck.** *Neuroimaging Clin N Am* 2016;26:259–78 CrossRef Medline
4. Anil G, Tan TY. **Imaging characteristics of schwannoma of the cervical sympathetic chain: a review of 12 cases.** *AJNR Am J Neuroradiol* 2010;31:1408–12 CrossRef Medline
5. Ota Y, Naganawa S, Kurokawa R, et al. **Assessment of MR imaging and CT in differentiating hereditary and nonhereditary paragangliomas.** *AJNR Am J Neuroradiol* 2021;42:1320–26 CrossRef Medline
6. Williams MD. **Paragangliomas of the head and neck: an overview from diagnosis to genetics.** *Head Neck Pathol* 2017;11:278–87 CrossRef Medline
7. Behuria S, Rout TK, Pattanayak S. **Diagnosis and management of schwannomas originating from the cervical vagus nerve.** *Ann R Coll Surg Engl* 2015;97:92–97 CrossRef Medline
8. Griffith B, Jain R. **Perfusion imaging in neuro-oncology: basic techniques and clinical applications.** *Radiol Clin North Am* 2015;53:497–511 CrossRef Medline
9. Cuenod CA, Balvay D. **Perfusion and vascular permeability: basic concepts and measurement in DCE-CT and DCE-MRI.** *Diagn Interv Imaging* 2013;94:1187–1204 CrossRef Medline
10. Gaddikeri S, Hippe DS, Anzai Y. **Dynamic contrast-enhanced MRI in the evaluation of carotid space paraganglioma versus schwannoma.** *J Neuroimaging* 2016;26:618–25 CrossRef Medline
11. Yuan Y, Shi H, Tao X. **Head and neck paragangliomas: diffusion weighted and dynamic contrast enhanced magnetic resonance imaging characteristics.** *BMC Med Imaging* 2016;16:12 CrossRef Medline

12. Gaddikeri S, Gaddikeri RS, Tailor T, et al. **Dynamic contrast-enhanced MR imaging in head and neck cancer: techniques and clinical applications.** *AJNR Am J Neuroradiol* 2016;37:588–95 CrossRef Medline

13. Ota Y, Liao E, Kurokawa R, et al. **Diffusion-weighted and dynamic contrast-enhanced MRI to assess radiation therapy response for head and neck paragangliomas.** *J Neuroimaging* 2021 May 8. [Epub ahead of print] CrossRef Medline

14. Srinivasan A, Dvorak R, Perni K, et al. **Differentiation of benign and malignant pathology in the head and neck using 3T apparent diffusion coefficient values: early experience.** *AJNR Am J Neuroradiol* 2008;29:40–44 CrossRef Medline

15. Koontz NA, Wiggins RH 3rd. **Differentiation of benign and malignant head and neck lesions with diffusion tensor imaging and DWI.** *AJR Am J Roentgenol* 2017;208:1110–15 CrossRef Medline

16. Landis JR, Koch GG. **The measurement of observer agreement for categorical data.** *Biometrics* 1977;33:159 CrossRef Medline

17. Offergeld C, Brase C, Yaremchuk S, et al. **Head and neck paragangliomas: clinical and molecular genetic classification.** *Clinics (Sao Paulo)* 2012;67:19–28 CrossRef Medline

18. Papiez J, Rojiani MV, Rojiani AM. **Vascular alterations in schwannoma.** *Int J Clin Exp Pathol* 2014;7:4032–38 Medline

19. Sourbron SP, Buckley DL. **On the scope and interpretation of the Tofts models for DCE-MRI.** *Magn Reson Med* 2011;66:735–45 CrossRef Medline

20. Zhao M, Guo LL, Huang N, et al. **Quantitative analysis of permeability for glioma grading using dynamic contrast-enhanced magnetic resonance imaging.** *Oncol Lett* 2017;14:5418–26 CrossRef Medline

21. Tischler AS, deKrijger RR. **15 years of paraganglioma: pathology of pheochromocytoma and paraganglioma.** *Endocr Relat Cancer* 2015;22:T123–33 CrossRef Medline